Higher thrust-to-power with large electrode gap spacing electroaerodynamic devices for aircraft propulsion

Haofeng Xu[1], Nicolas Gomez-Vega[1], Devansh R. Agrawal[1] and Steven R. H. Barrett[1]

[1]Department of Aeronautics and Astronautics, Massachusetts Institute of Technology, Cambridge, MA 02139, USA

E-mail: `sbarrett@mit.edu`

Abstract. Electroaerodynamic (EAD) devices, which produce a propulsive force in air by electrostatic acceleration, have been demonstrated as a method of propulsion for airplanes. However, achieving sufficient thrust-to-power is a significant challenge in developing EAD aircraft which are practical. Theory predicts that devices with larger inter-electrode gap spacing will enable higher thrust-to-power, but most experimental work has been limited to gap spacings of less than 80 mm. Those studies which have investigated spacings of greater than 100 mm have found results deviating from theory, with lower thrust-to-power than predicted. We performed experiments between 50 and 300 mm gap spacing, and conclude that three effects explain the discrepancy: "leakage current" from the electrodes to the surroundings, which does not produce thrust but increases measured electrical power; reverse corona emission from the collecting electrode, which reduces thrust and increases power; and the electric potential of the thruster relative to its surroundings, which affects both leakage current and reverse corona emission. Our results show that if these effects are accounted for, the existing EAD theory is correct without modification beyond its previous range of validity, and is applicable to wire-to-cylinder EAD devices up to at least 300 mm gap spacing. We support our experimental results with two-dimensional numerical simulations, which show that the experimental current and thrust, including effects of leakage current, can be reproduced by computation with 12 % error – an important step towards numerical design and optimization. By experimentally replicating equilibrium in-flight conditions, we measure thrust-to-power in the laboratory of up to 15 N/kW for large gap spacing thrusters at practically useful thrust levels. This is two to three times higher than current implementations with smaller gap spacings, suggesting that large gap spacing thrusters will be suitable for future EAD-propelled flight applications at thrust-to-power competitive with or exceeding conventional propulsion.

Keywords: Electroaerodynamics, Electrohydrodynamics, Plasma Physics

Submitted to: *J. Phys. D: Appl. Phys.*

1. Introduction

Electroaerodynamic (EAD) devices are a means to generate propulsive forces in fluids without any moving parts. These devices use an electric field to produce ions in a neutral fluid such as air, and then accelerate these ions by the Coulomb force. Collisions between the ions and neutral molecules transfer momentum from the ions to the bulk fluid and result in an "ionic wind". Ionic winds have been studied for applications such as solid-state pumping [1, 2], heat transfer enhancement [3, 4], and flow-control [5, 6, 7]. Most EAD devices produce and accelerate ions in a neutral fluid using a corona discharge, which is a type of self-sustained glow discharge created by applying a steady state direct current (DC) voltage across two asymmetric electrodes. There are also EAD devices which operate using pulsed and alternating current (AC) discharges. In particular, the AC dielectric barrier discharge (DBD), whose geometry can be integrated into the surface of an airfoil, is being studied for aerodynamic flow control applications [6, 8, 9].

EAD devices and the ionic winds which they produce have also been proposed as a method of propulsive force-generation for aircraft, either as a "lifter" [10, 11], or as a forward propulsor [12, 13, 14, 15]. Conventional aircraft propulsion systems which are used for lift and forward propulsion rely on moving aerodynamic surfaces, such as propellers and gas turbines, to produce thrust. EAD is an alternative which directly converts electrical energy to mechanical energy in the airflow, with no need for moving surfaces. The motivation for developing such a "solid-state", fully electric thrust production system is threefold: it is quieter, mechanically simpler, and emits no direct combustion emissions (although ozone is produced in the ionization process). Therefore, an EAD propulsion system could potentially reduce the noise and air pollution produced by conventional propulsion systems and in the near term may find applications in drones, particularly those operating in urban environments. Moreover, the different physical processes of EAD propulsion, governed by different scaling laws and constraints to conventional propulsion, could enable flight at scales and with configurations that are not possible now. For example, the potential for EAD aircraft at the sub-centimeter scale is already being explored [10].

The first peer-reviewed study of EAD devices for propulsion applications was by Christensen and Moller in 1967 [16], who concluded that orders of magnitude improvement in performance would be required for EAD to be practical as a method of propulsion. In the following 50 years, theoretical and experimental analyses broadly confirmed these findings [12, 17, 15]. However, recent work, which optimized the thrust density [18] and applied modern power electronics design [19] and aircraft design optimization methods led to the demonstration of a flying EAD airplane [20]. This proof-of-concept demonstrated that EAD aircraft are feasible at the UAV scale, and could be suitable initially for applications where low noise and mechanical simplicity are valued above range, payload, and efficiency.

The proof-of-concept aircraft did not carry a payload and had a endurance of 90 seconds. Increasing the thrust-to-power, T/P, of the EAD propulsion system would

increase the aircraft-level payload and endurance of future EAD-propelled aircraft.

EAD theory predicts that at low speeds, the thrust, T, of an EAD thruster is

$$T = \frac{Id}{\mu}, \tag{1}$$

where I is the current between electrodes, d is the electrode gap spacing, and μ is the ion mobility of the ambient fluid. Equation 1 is derived by evaluating the Coulomb force on the ions travelling between two parallel plate electrodes [1, 16, 14], though Gilmore and Barrett [21] showed that it should also apply to other electrode geometries. The electrode where ions are produced is the emitter (usually the anode), and the other is the collector (usually the cathode).

In the idealized EAD drift theory, the ion mobility, $\mu = v_i/E$, which relates ion drift speed v_i and electric field strength E, is assumed to be uniform. Ion mobility is a function of the chemical composition of the working fluid, the fluid pressure, and the local electric field. The pressure is approximately constant for unducted atmospheric thrusters at sea level. The theoretical dependence on electric field strength is less than 5 % for electric field strengths below 5×10^5 V/m [22], as is the case here. Measurements of ion mobility from Moreau et al. [23] at different gap spacings showed variations of less than 10 %.

In addition to uniform ion mobility, the derivation of Equation 1 assumes that the current, I, is unipolar (i.e. consists only of ions of one polarity) and flows only from the emitter to the collector. We find that this assumption does not always hold: under certain conditions, a negative corona discharge can be formed at the cathode, resulting in the flow of negative ions from cathode to anode.

Moreover, idealized EAD theory does not account for aerodynamic effects. Equation 1 calculates the electrostatic force; however, the net force produced by an EAD device – and measured by experiments – will be reduced by aerodynamic drag on the electrodes. In static laboratory conditions, where flow velocities are low, the drag is small compared to the Coulomb force [24].

The thrust-to-power is defined as the thrust force divided by input electrical power

$$\frac{T}{P} = \frac{Id}{\mu} \cdot \frac{1}{IV_a} = \frac{d}{\mu V_a}, \tag{2}$$

where V_a is the applied voltage across the electrodes. The development of EAD devices with larger gap spacings, d, is therefore a path to higher thrust-to-power.

However, many past experiments have not quantified EAD performance at gap spacings greater than 80 or 100 mm [15, 21, 23, 25, 26, 27, 28]. The few experiments which do extend to larger gap spacings find unexpected results which show apparent deviation from one-dimensional theory and significantly worse performance [12, 14, 29]. For example, the observed deviation from idealized theory, especially at high gap spacings, was a contributing factor to Wilson et al.'s [12] conclusion that EAD was not practical for propulsion. Similarly, the results in Masuyama and Barrett [14], for gap spacings greater than 90 mm, showed a bi-linear degradation in thrust-to-power.

We performed experiments for large thrusters of up to 300 mm gap spacing, and found a number of physical effects not accounted for in the idealized theory, which reduce EAD thruster performance. We find methods to avoid or account for these non-ideal effects and accurately predict equilibrium in-flight EAD performance from laboratory experiments, relevant to developing practical large gap spacing, high thrust-to-power propulsion devices for flying aircraft.

We performed numerical simulations, applying more accurate boundary conditions to existing numerical methods, and are able to reproduce our experimental results, including the effect of non-ideal current leakage. These numerical methods can be used to perform rapid design and optimization of EAD thruster geometry.

2. Experimental Setup

We performed experiments with wire-to-cylinder EAD thrusters, applying a voltage across the electrodes and measuring the current and thrust force. The span of the emitter was 750 mm, which is wider than all known previous experiments. The collector was 100 mm longer than the emitter, which reduces corona emission at the electrode ends.

The thruster consisted of a rectangular glass fiber reinforced polymer (GFRP) frame which held the emitting and collecting electrodes. The emitter was a 0.254 mm tungsten wire, which offers high erosion resistance in coronas [30]. The collector was a thin-walled aluminum cylinder with a diameter of either 9.5, 12.7, 19.1, 25.4, or 38.1 mm.

A voltage was applied to the the electrodes using bench-top high voltage DC power supplies. Insulated wire (28 AWG stranded wire with fluorinated ethylene propylene insulation) was used to connect the high voltage outputs to the thruster electrodes.

We used two DC bench-top high voltage power supplies of different polarities either individually or in combination (Figure 1). The positive polarity supply (Matsusada AU120-P) biases its output positive to ground, and the negative polarity supply (Matsusada AU-120-N) biases its output negative to ground. This allowed the setting of the potentials of the emitter and collector relative to each other, as well as the potential of both electrodes relative to the grounded surroundings of the experiment.

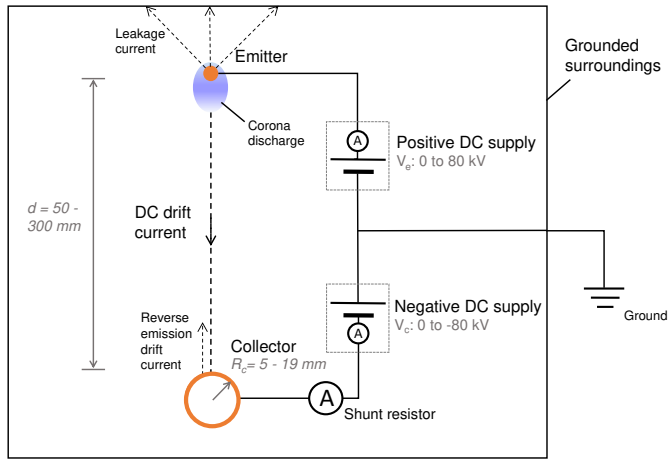

Figure 1. Electrical schematic of experimental setup. End view of electrodes. Some experiments used the positive DC supply only. Power supplies have internal current and voltage measurement. An independent shunt resistor is used to measure current through the collector when the negative DC supply is not used. Not to scale.

We define V_a as the applied voltage across the electrodes, V_e as the voltage of the emitter relative to ground, and $V_c \leq 0$ as the voltage of the collector relative to ground. Therefore $V_a = V_e - V_c$.

In sections 3.1 and 3.2, where we quantify the effects of leakage current and reverse emission, only the positive supply is used (i.e. $V_e = V_a$ and $V_c = 0$).

In section 3.3, both supplies are used to quantify the effect of the relative potential to the experimental surroundings. We set $V_e = \alpha V_a$ and $V_c = (1 - \alpha)V_a$, where α is varied between 0 and 1. For example, for inter-electrode voltage $V_a = 80\,\mathrm{kV}$ with $\alpha = 0.5$ (symmetric differential mode), the output of the positive supply (and hence the emitter) would be at $40\,\mathrm{kV}$ and the output of the negative supply (and the collector) would be at $-40\,\mathrm{kV}$ relative to ground.

The power supplies had internal current and voltage measurements, taken at the high voltage output. These internal current and voltage measurements were calibrated using a shunt resistor and a Tektronix P6015A high voltage probe respectively, and both were accurate to within 1 %.

An independent current measurement was made at the collector to measure only the current between the electrodes, and not the leakage current to the surroundings. We measured the voltage across a $6.8\,\Omega$ shunt resistor, multiplied with an operational amplifier [31]. This was used in sections 3.1 and 3.2 when the negative supply was not connected and $V_c = 0$. The constant resistor value was chosen to give voltage readings within the measurement range of our multimeter.

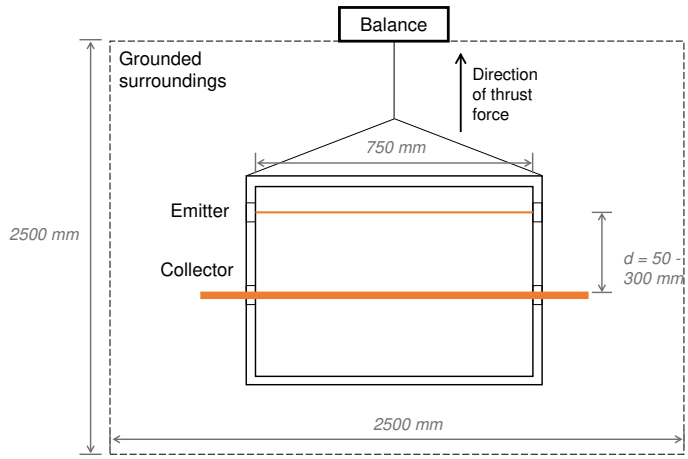

Figure 2. Schematic of thruster and thrust measurement setup. Side view of electrodes. Not to scale.

We measured thrust by hanging the thruster vertically from a scale and recording the change in force measured by the scale (Figure 2). The scale was a Sartorius Entris 4202 balance with 10 mg resolution. The experimental space measured 3 m wide by 2.5 m long. The scale was supported 2.5 m from the floor by a GFRP cantilevered truss, and the thruster suspended from the scale by a nylon line. The experimental volume was evacuated of all conducting elements, except for the thruster itself and the high voltage cables, which were insulated to a rated 120 kV.

This experimental space is larger than those used in similar experiments, and reduces the effect of the surrounding elements on the electric field. In our two-dimensional numerical model, the ground boundary condition is a rectangular boundary of 2.5 m long by 2.5 m high, matching the cross section of the experimental setup.

In our experiments, the emitter-collector voltage V_a was increased in steps of 2 kV. The upper limit of the applied voltage was at 80 kV or at the onset of arcing, whichever was lower. Voltage, current, and thrust measurements were recorded simultaneously at a frequency of 25 Hz. Thrust and current data were normalized by the emitter span.

Temperature and relative humidity were measured using an Omega HH311 probe. Experiments were conducted at room conditions, at a temperature of approximately 24 °C and relative humidity ranging from 33 % to 52 %. The relative humidity can affect the ion mobility of air [32], though we do not observe any effect in this range of relative humidities. This is in agreement with other EAD experiments [23].

Each data point plotted is the mean of approximately 400 data points recorded over a period of 15 seconds. The standard deviation for the thrust was less than 3 mN/m; the maximum error was 2.5 %.

3. Experimental Results

The experimental results are divided into four sections. Each of the first three addresses a separate experimental effect that we found, while the final section presents predictive thrust performance results for EAD thrusters in flight.

3.1. Effect of Leakage Current

Measuring the current flowing through the collector using an independent shunt resistor showed a difference between the currents measured at the emitter and collector, indicating that current originating from the emitter does not all flow to the collector (Figure 3(a)). The current flowing by another path, which we term "leakage current", had been previously observed by Monrolin et al. [15] and was attributed to corona discharge at the electrode connections. The current which does flow from emitter to the collector we term the "corrected current".

Figure 3(b) shows that the discharge characteristic of the leakage current is consistent with that of a corona discharge, with an inception voltage, V_0, of approximately 20 kV. The inception voltage for the leakage current is approximately the same as the inception voltage for the primary emitter-collector current, suggesting that the the leakage current also originates from the emitter itself (as opposed to the electrode connections or the GFRP frame for example).

The leakage current varies weakly with the gap spacing. Increasing the gap spacing from 100 mm to 300 mm increases the leakage current from 0.015 mA/m to 0.018 mA/m. This suggests that the leakage current is primarily driven by the electric field between the emitter and the surrounding ground, and not the electric field between the emitter and the collector.

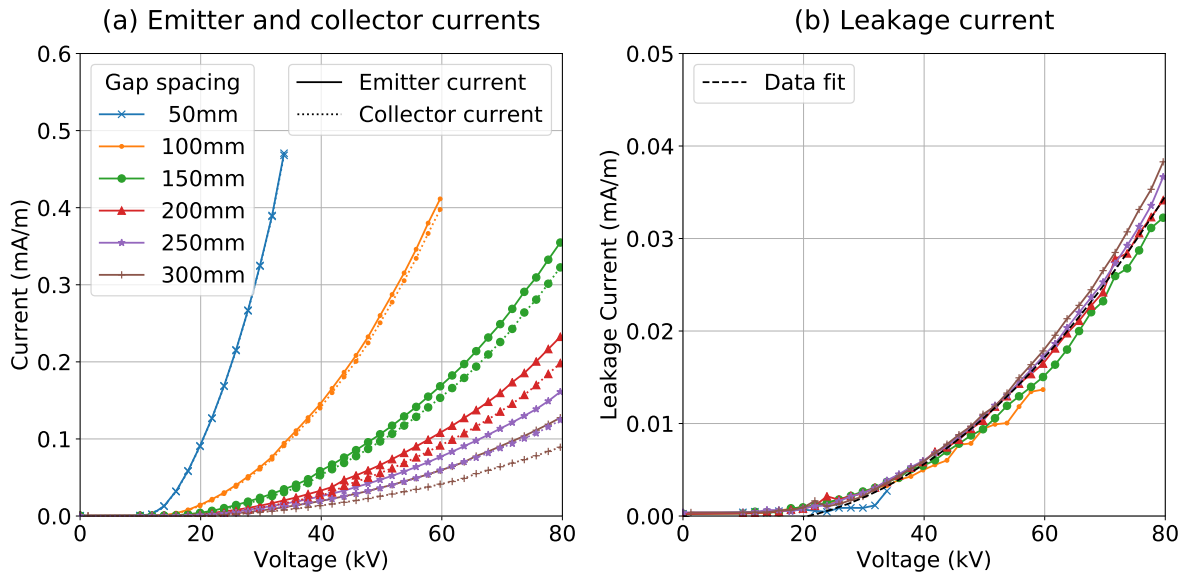

Figure 3. (a) Current vs. voltage at varying gap spacings. Solid lines are emitter current and dashed lines are collector current. (b) Leakage current, which is the difference between the solid lines and the dashed lines in panel a), flows from the emitter to the grounded surroundings. A data fit of the form $I = CV_a(V_a - V_0)$ is shown, with $C = 7.3 \times 10^{-6}\,\mathrm{mAkV^{-2}m^{-1}}$, $V_0 = 20.8\,\mathrm{kV}$. Note the different y-axis scales. The collector diameter is 38 mm. Only the positive power supply is used ($V_e = V_a$ and $V_c = 0$). The collector is connected to ground through a $6.8\,\Omega$ current measurement resistor, and the negative supply is not used.

Figure 4(a) shows thrust vs $I_{\mathrm{total}} \cdot d$. From Equation 1, we expect straight lines of slope $1/\mu$. At larger gap spacings, where the leakage current is a larger fraction of the total current, using the total current rather than the corrected current results in an apparent deviation from theory, with a higher effective ion mobility at larger gap spacings. This results in reduced thrust-to-power performance at larger gap spacings than expected from Equation 2.

Figure 4(b) shows that when the corrected current is used instead, the measured gradient $1/\mu$ is independent of gap spacing and implies an ion mobility of $2.43 \times 10^{-4}\,\mathrm{m^2V^{-1}s^{-1}}$. The degradation observed in Figure 4(a) is due to the inclusion of leakage current rather than an actual change in ion mobility at larger gap spacings.

Figure 4(b) also suggests that leakage current does not have a significant effect on thrust. Once corrected for leakage current, the thrust performance is unaffected. The performance degradation is only through increased power draw at the power supply, and not thrust decrease.

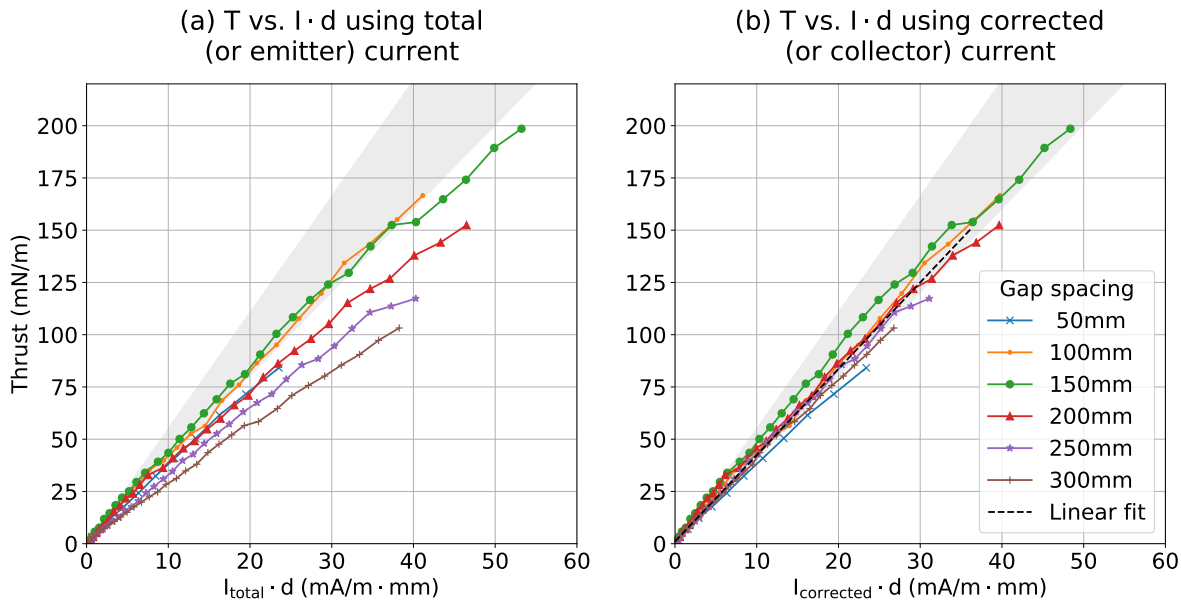

Figure 4. Thrust vs. the product of current and gap spacing at different gap spacings, with (a) total drawn current and (b) corrected current. Shaded regions show the range of reported ion mobilities for air: $1.8 \times 10^{-4} \leq \mu \leq 2.5 \times 10^{-4}\,\mathrm{m^2V^{-1}s^{-1}}$ [33, 34]. Linear fit in (b) shows an average measured ion mobility $2.43 \times 10^{-4}\,\mathrm{m^2V^{-1}s^{-1}}$. The collector diameter is 38 mm. The lower measured thrust for the 50 mm case is attributed to flow blockage and increased aerodynamic drag at the low gap spacing.

3.2. Effect of Collector Diameter and Reverse Emission

We find that while leakage current effects allow us to recover the predictions of EAD theory, this is only true at large collector electrode diameters.

Figure 5 shows that for smaller collector diameters, (a) a lower thrust is produced at the same voltage and gap spacing, and (b) a higher corrected current per unit thrust is measured (the gap spacing is the same for all runs).

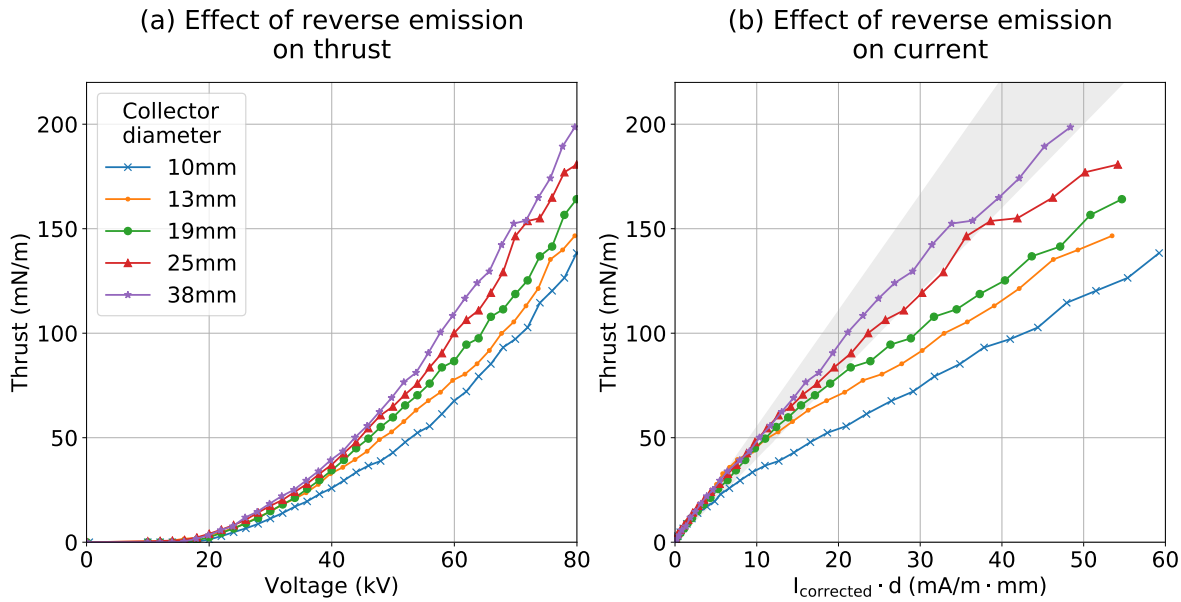

Figure 5. (a) Thrust vs. voltage (b) thrust vs. the product of current and gap spacing at 150 mm gap spacing for varying collector diameters. Lower thrust and higher current draw for smaller collector diameters is consistent with reverse corona emission at the collector electrode.

These results suggest the presence of another non-ideal effect: reverse corona emission at the collector. The assumption of unipolar ion drift relies on ions being produced solely in a region close to the emitter. However, if the electric field at the collector becomes sufficiently high that a corona discharge forms there, this is no longer the case. Negative ions formed at the collector are accelerated towards the emitter under the effect of the applied voltage. These negative ions produce thrust opposite to the positive ions, reducing the net thrust; they add to the current and increase the power draw.

This reverse emission or bipolar conduction effect had been previously observed [14, 15]. We find that it can be mitigated by increasing the collector diameter. Figure 5(b) shows that reverse emission (and deviation from idealized theory) occurs at higher voltages for larger collectors, consistent with the higher corona inception voltage for larger radius electrodes. A larger radius of curvature results in lower local electric field. For the largest 38 mm collector, there is no observed reverse emission in the tested range of voltages.

Reverse emission has a significant impact on thrust-to-power. At 80 kV, reverse emission reduces the thrust for the 10 mm collector by more than 30 % compared with the larger 38 mm collector, and increases power draw by 25 %. As a result, the thrust-to-power is almost halved. Reverse emission is a problem for larger gap spacing devices where the applied voltages are higher: while a 13 mm collector is sufficient to avoid reverse emission at 40 kV, a much larger 38 mm collector is needed at 80 kV.

Large collectors pose a design challenge for aircraft both in terms of weight and aerodynamic drag, in particular at higher flight velocities. This motivates the

development of methods to accurately predict reverse emission and optimize the geometry of collectors to have low drag while keeping the electric field below the corona inception value.

3.3. Effect of Boundary Potential

An experimental parameter whose effect has not been previously quantified is the voltage bias of the thruster relative to its surroundings in the experimental room. All previous EAD experiments with the positive corona (including those in the preceding sections) have used a positive power supply to bias the emitter positive relative to ground, while the collector is held at ground potential.

Figure 6(a) shows the thrust measured using this conventional configuration compared with other power supply configurations where the relative voltage between the thruster and ground is more negative. The relative voltage between emitter and collector is the same in all the cases. When the thruster is at a more negative potential with respect to ground, the thrust is lower. In the extreme case where the emitter is at ground and the collector is negative at $-V_a$, the thrust is lower by 25 %. We also observe signs of reverse emission for $V_e = 0$ and $V_e = 0.25V_a$, whereas we do not observe them for $V_e = V_a$, even though the collector diameter is the same 38 mm.

Changing the potential of the experimental boundary changes the electric field distribution around the thruster, and therefore its current and thrust characteristics. It is conventionally assumed that the grounded boundary sufficiently far away from the thruster that it has no effect. For our experimental space which is at least 2.5 m in each dimension, the results in Figure 6 show that this assumption does not hold. The potential of the thruster relative to its surroundings should therefore be controlled.

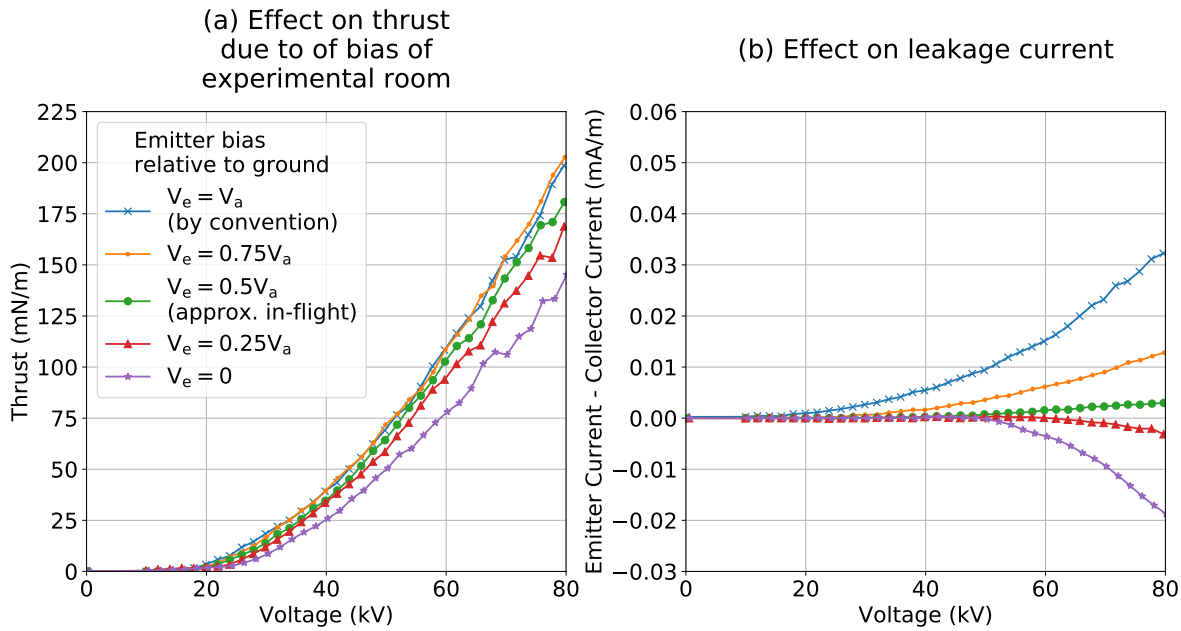

Figure 6. (a) Thrust and (b) leakage current against voltage for varying power supply biases. $V_e = V$ and $V_e = 0$ represent the emitter-positive-collector-ground, and collector-negative-emitter-ground cases respectively. All the configurations have the same relative voltage between emitter and collector. The leakage current is the emitter current minus the collector current. Negative values of leakage current means that current is flowing from the collector to the grounded surroundings due to corona emission occurring at the collector. The gap spacing is 150 mm and the collector diameter is 38 mm

Figure 6(b) shows that leakage current changes depending on the potential of the thruster relative to its surroundings. When the emitter is biased fully positive relative to the surroundings ($V_e = V$), we observe the same corona-like leakage current that was seen in Figure 3. When the collector is biased negative relative to the surroundings ($V_e = 0$), we find that the current at the collector is higher than that at the emitter, suggesting that there is corona leakage current flowing from the collector to the experimental surroundings (this is a current of negatively charged ions).

For the intermediate cases, when the emitter is biased partly positive to ground, and the collector partly negative to ground, the leakage current is smaller. The leakage current is approximately zero in the differential configuration where V_e is $0.5V_a$. While a number of factors affect the charge of an aircraft in-flight [35], and hence its potential relative to its surroundings, we use the differential configuration to approximate an equilibrium condition where there is approximately zero net current emitted by the aircraft.

3.4. Thrust-to-power at Gap Spacings Greater Than 100 mm

We performed experiments in the differential configuration ($V_e = 0.5V$) over a range of gap spacings; measurements of the expected thrust-to-power in this equilibrium

condition are shown in Figure 7.

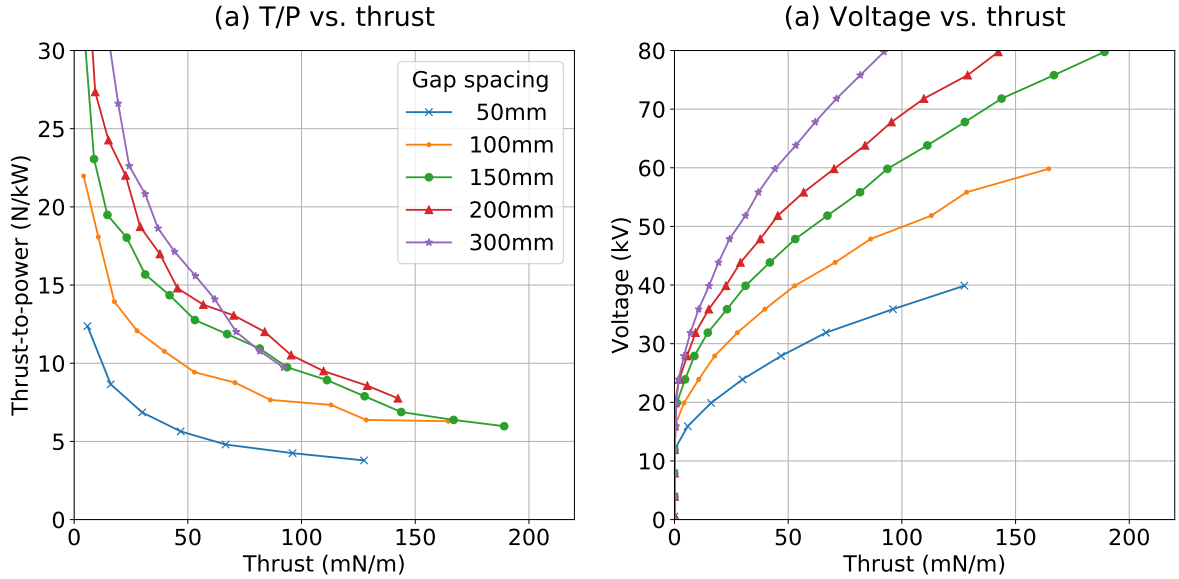

Figure 7. (a) Thrust-to-power versus thrust, and (b) voltage versus thrust for different gap spacings using a differential $V_e = 0.5V_a$ power supply configuration and a 38 mm collector. Power is calculated using the total drawn current, which is the maximum current recorded at either electrode. In differential mode, the net leakage current is approximately zero, and the measured difference between the emitter and collector currents is less than 2 % in all cases.

Figure 7(a) shows that increasing gap spacing increases thrust-to-power at a given thrust. At 200 mm gap spacing, a thrust-to-power of 10 N/kW is achievable for a thrust per unit span of 100 mN/m. This is higher than the 7.5 N/kW achieved at 100 mm spacing and 4.5 N/kW at 50 mm spacing for the same thrust level. The caveat, shown in Figure 7(b), is that to produce the same thrust of 100 mN/m, 70 kV is needed for 200 mm gap spacing, while 50 kV for 100 mm gap spacing. Provided this higher voltage can be supplied, higher thrust-to-power of large gap spacing thrusters could enable longer range and endurance at the aircraft level.

4. Electrostatic Modeling

Computational modeling of EAD thrusters enables rapid design and assessment. Numerical models developed in the context of electrostatic precipitators have simulated corona discharge devices [36, 37]. Recent studies have applied these methods to EAD propulsion [38, 39, 40] to calculate current and thrust characteristics, though numerical results were not experimentally validated. We applied the numerical scheme developed by Davis and Hoburg [37] to our EAD device and were able to reproduce the experimentally observed leakage current effect.

4.1. Numerical Scheme and Boundary Conditions

We used the iterative numerical scheme described in Davis and Hoburg [37]. In steady state, the governing equations solved are Gauss's Law and charge conservation,

$$\nabla^2 V = -\rho_c/\epsilon_0, \tag{3}$$

$$\nabla \cdot \vec{j} = \nabla \cdot (\rho_c \mu \vec{E}) = 0, \tag{4}$$

where V is the electrostatic potential, ρ_c is the space charge density, $\vec{j}$ is the current density, and ϵ_0 is the permittivity of free space. The boundary conditions were specified by voltage on the emitter surface ($V = V_e = 80\,\mathrm{kV}$), voltage on collector surface ($V = V_c = 0$), and voltage on the bounding box ($V = V_b = 0$). Equations 3 and 4 were solved using a finite element method ($\sim$ 130,000 triangular elements, converged to 0.5 % RMS error) and the method of characteristics ($\sim$ 300 characteristics) respectively [37]. Consistent with Kaptsov's condition [41], the scheme was iteratively solved for the initial space charge until the mean electric field magnitude at the emitter converged to Peek's formula for corona inception [42]. The critical field used was $8.66 \times 10^6\,\mathrm{V/m}$, and the ion mobility used was our experimentally measured value of $2.4 \times 10^{-4}\,\mathrm{m^2V^{-1}s^{-1}}$ (from Figure 4(b)). Grid convergence was established since tripling number of mesh elements and doubling tolerance requirements changed results by less than 5 %.

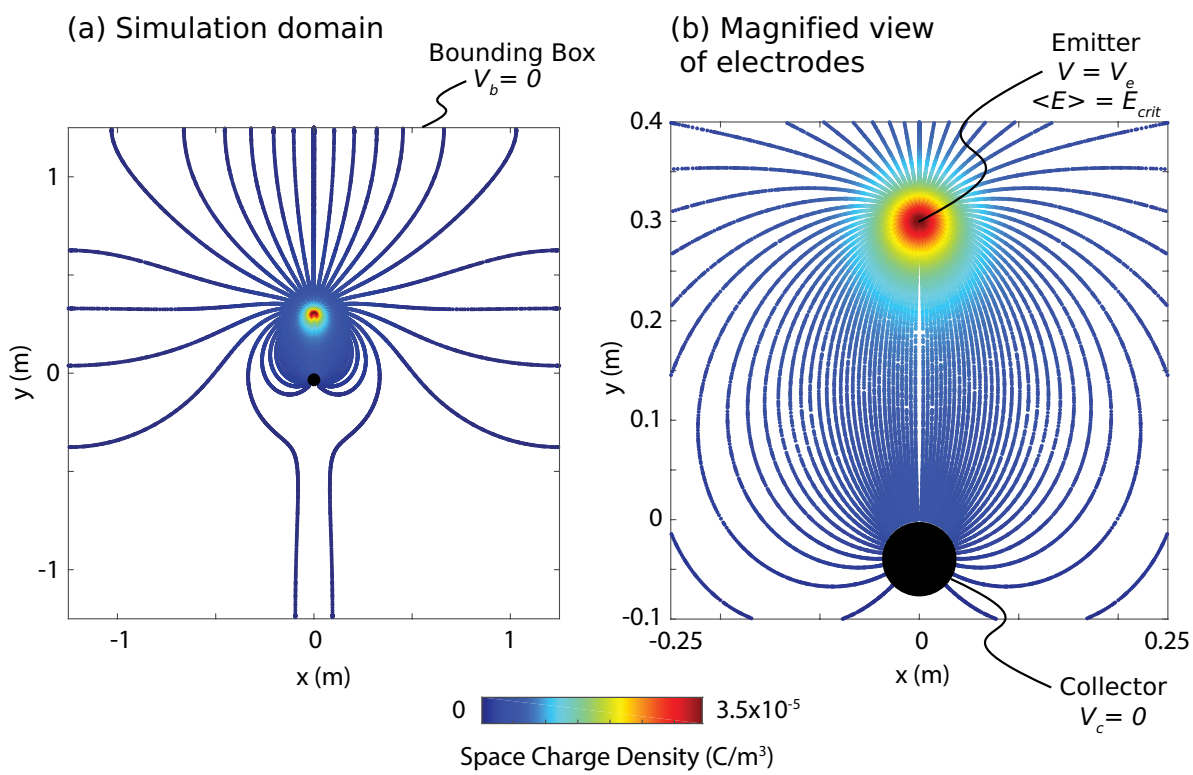

Figure 8. (a) Entire simulation domain and (b) magnified view of electrodes, showing current paths. Large black circle is the collector. Boundary conditions are indicated. Simulation conditions: V_e=80 kV, V_c=0 kV, V_b=0 kV, d=300 mm, $2r_c$=38 mm.

The modeling assumptions and boundary conditions were different to previous studies, but consistent with our experimental setup: i) the computational domain corresponded to our experimental area, which was 2.5 m by 2.5 m (Figure 8). This was larger than previous numerical studies [38, 39, 40] where the size of the computational domain was in the order of centimeters; ii) the voltage of the boundary was set at ground; and (iii) characteristic lines (and hence current flow) from the emitter to the boundary were permitted.

4.2. Results

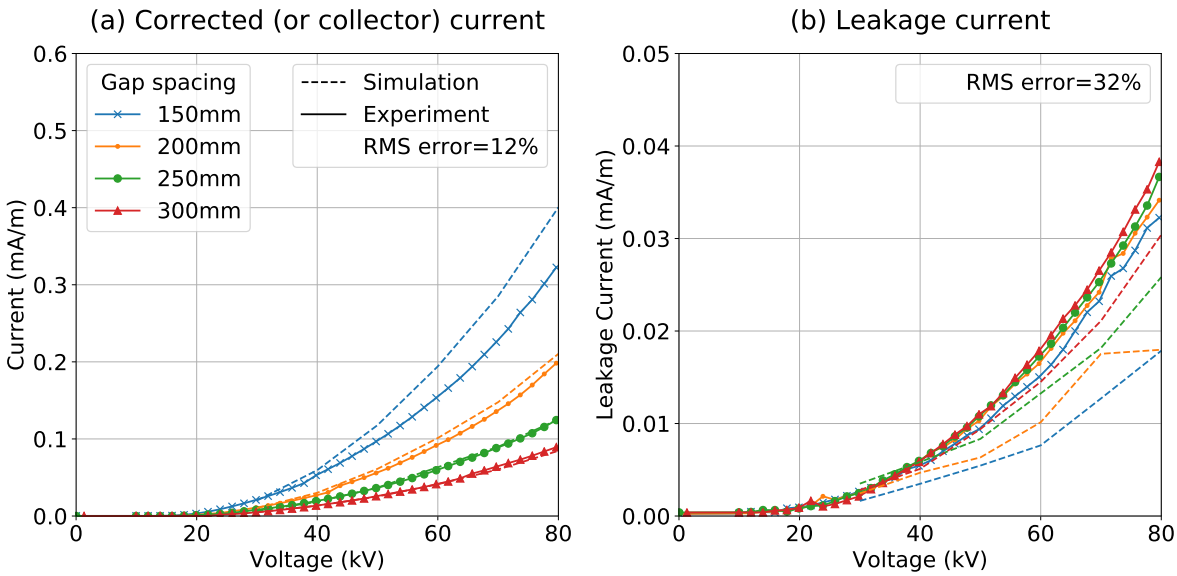

Figure 9. Experimental and numerical results for (a) corrected current (which is the current measured at the collector) and (b) leakage current. Results obtained by matching the boundary conditions and electrode potentials in simulations to those in experiment.

Figure 9(a) shows that the numerical scheme is able to reproduce the discharge characteristics of the EAD device over a range of voltages and gap spacings. The RMS error for the corrected current is 12 %. Prediction of corrected current enables improved prediction of thrust; experimental results show that the thrust is approximately proportional to corrected current, consistent with Equation 1 (Figure 4(b)).

The non-ideal effect of leakage current is also captured by our model, since current is permitted to from the emitter to the bounding box in the simulation. Figure 9(b) shows that the simulated leakage current is consistent with measured values, in particular for high gap spacings. These results support our hypothesis that the greater part of the leakage current originates from the emitter itself, and not the electrode connections. Since the magnitude of leakage current is about 10 times smaller than the total emitter current, the simulation errors are proportionately larger at 32 %.

5. Conclusions

EAD thruster experiments with different geometries and electrical parameters have elucidated two primary non-ideal effects associated with EAD thrusters: current leakage to the surroundings in static experimental conditions and reverse emission from the collector, which may be relevant in flight. A factor previously not considered in experiments, the bias of the thruster relative to its surroundings, is found to influence these two non-ideal effects.

Leakage current is an experimental effect not expected in-flight (expect potentially near the ground). It can can be mitigated by performing experiments with power supplies in a differential configuration, where the voltage of the emitter relative to the grounded experimental surroundings is $0.5V_a$, and that of the collector, $-0.5V_a$.

Reverse emission is a phenomenon which degrades EAD thruster performance, especially at higher voltages. It is affected by the power supply configuration, but primarily determined by geometrical electrode design. It can be avoided by sizing the collector so that at the operating voltage, the maximum field at the collector is lower than the critical corona field.

Following procedures to minimize leakage current and prevent reverse emission, we are able to show that large gap spacing EAD devices can have higher thrust-to-power than existing smaller gap spacing devices. Increasing the gap spacing from the present 50 mm to a larger 200 or 300 mm could increase the thrust-to-power up to two or three-fold.

Overall, these experimental results show that the predictions of canonical EAD theory (Equations 1 and 2) hold outside the previously observed range of validity, and that previously observed deviations can be explained without modification to the theory.

In the design of EAD aircraft, it is necessary to develop numerical methods to predict the electrical performance of different electrode geometries, and balance the competing requirements of preventing reverse emission and reducing aerodynamic drag. Our first steps in numerical modeling are able to predict the current (and hence thrust) to within 12 % of experimentally measured values, as well as reproduce the experimentally observed effect of leakage current. These models will be an important tool in rapid future EAD device design and optimization.

6. Acknowledgements

This work was funded through the Professor Amar G. Bose Research Grant.

7. References

[1] Otmar M. Stuetzer. Ion drag pressure generation. *Journal of Applied Physics*, 30(7):984–994, jul 1959.

[2] William F. Pickard. Ion drag pumping. I. theory. *Journal of Applied Physics*, 34(2):246–250, February 1963.

[3] M. E. Franke and L. E. Hogue. Electrostatic cooling of a horizontal cylinder. *Journal of Heat Transfer*, 113(3):544, 1991.

[4] N.E. Jewell-Larsen, E. Tran, I.A. Krichtafovitch, and A.V. Mamishev. Design and optimization of electrostatic fluid accelerators. *IEEE Transactions on Dielectrics and Electrical Insulation*, 13(1):191–203, feb 2006.

[5] Eric Moreau. Airflow control by non-thermal plasma actuators. *Journal of Physics D: Applied Physics*, 40(3):605–636, jan 2007.

[6] C. L. Enloe, Thomas E. McLaughlin, Robert D. Van Dyken, K. D. Kachner, Eric J. Jumper, and Thomas C. Corke. Mechanisms and responses of a single dielectric barrier plasma actuator: Plasma morphology. *AIAA Journal*, 42(3):589–594, mar 2004.

[7] J. Reece Roth. Aerodynamic flow acceleration using paraelectric and peristaltic electrohydrodynamic effects of a one atmosphere uniform glow discharge plasma. *Physics of Plasmas*, 10(5):2117–2126, may 2003.

[8] Thomas C. Corke, Martiqua L. Post, and Dmitriy M. Orlov. Single dielectric barrier discharge plasma enhanced aerodynamics: physics, modeling and applications. *Experiments in Fluids*, 46(1):1–26, nov 2008.

[9] Nicolas Benard and Eric Moreau. Electrical and mechanical characteristics of surface AC dielectric barrier discharge plasma actuators applied to airflow control. *Experiments in Fluids*, 55(11), nov 2014.

[10] Daniel S. Drew, Nathan O. Lambert, Craig B. Schindler, and Kristofer S. J. Pister. Toward controlled flight of the ionocraft: A flying microrobot using electrohydrodynamic thrust with onboard sensing and no moving parts. *IEEE Robotics and Automation Letters*, 3(4):2807–2813, oct 2018.

[11] Vladislav Yu. Khomich and Igor E. Rebrov. In-atmosphere electrohydrodynamic propulsion aircraft with wireless supply onboard. *Journal of Electrostatics*, 95:1–12, oct 2018.

[12] J. Wilson, H. D. Perkins, and W. K. Thompson. An investigation of ionic wind propulsion. Technical Report TM-2009-215822, NASA, 2009.

[13] Ho Shing Poon, Mark K. K. Lam, Maxwell Chow, and Wen J. Li. Noiseless and vibration-free ionic propulsion technology for indoor surveillance blimps. In *2009 IEEE International Conference on Robotics and Automation*. IEEE, may 2009.

[14] K. Masuyama and S. R. H. Barrett. On the performance of electrohydrodynamic propulsion. *Proceedings of the Royal Society A: Mathematical, Physical and Engineering Sciences*, 469(2154):20120623–20120623, apr 2013.

[15] N. Monrolin, F. Plouraboué, and O. Praud. Electrohydrodynamic thrust for in-atmosphere propulsion. *AIAA Journal*, 55(12):4296–4305, dec 2017.

[16] E. A. Christensen and P. S. Moller. Ion-neutral propulsion in atmospheric media. *AIAA Journal*, 5(10):1768–1773, oct 1967.

[17] L. Pekker and M. Young. Model of ideal electrohydrodynamic thruster. *Journal of Propulsion and Power*, 27(4):786–792, jul 2011.

[18] Christopher K. Gilmore. *Electro-aerodynamic thrust for fixed-wing aircraft propulsion*. PhD thesis, Massachusetts Institute of Technology, 2016.

[19] Yiou He, Mark Woolston, and David Perreault. Design and implementation of a lightweight high-voltage power converter for electro-aerodynamic propulsion. In *2017 IEEE 18th Workshop on Control and Modeling for Power Electronics (COMPEL)*. IEEE, jul 2017.

[20] Haofeng Xu, Yiou He, Kieran L. Strobel, Christopher K. Gilmore, Sean P. Kelley, Cooper C. Hennick, Thomas Sebastian, Mark R. Woolston, David J. Perreault, and Steven R. H. Barrett. Flight of an aeroplane with solid-state propulsion. *Nature*, 563(7732):532–535, nov 2018.

[21] C. K. Gilmore and S. R. H. Barrett. Electrohydrodynamic thrust density using positive corona-induced ionic winds for in-atmosphere propulsion. *Proceedings of the Royal Society A: Mathematical, Physical and Engineering Sciences*, 471(2175):20140912–20140912, feb 2015.

[22] Christopher K. Gilmore and Steven R.H. Barrett. Electroaerodynamic thruster performance as a

function of altitude and flight speed. *AIAA Journal*, 56(3):1105–1117, mar 2018.

[23] Eric Moreau, Nicolas Benard, Jean-Daniel Lan-Sun-Luk, and Jean-Pierre Chabriat. Electrohydrodynamic force produced by a wire-to-cylinder dc corona discharge in air at atmospheric pressure. *Journal of Physics D: Applied Physics*, 46(47):475204, oct 2013.

[24] Lin Zhao and Kazimierz Adamiak. Numerical analysis of forces in an electrostatic levitation unit. *Journal of Electrostatics*, 63(6-10):729–734, jun 2005.

[25] Konstantinos N. Kiousis, Antonios X. Moronis, and Wolf G. Fruh. Electro-hydrodynamic (EHD) thrust analysis in wire-cylinder electrode arrangement. *Plasma Science and Technology*, 16(4):363–369, apr 2014.

[26] Eric Moreau, Nicolas Benard, Frédéric Alicalapa, and Alexandre Douyère. Electrohydrodynamic force produced by a corona discharge between a wire active electrode and several cylinder electrodes – application to electric propulsion. *Journal of Electrostatics*, 76:194–200, aug 2015.

[27] D V Dremin, V Yu Khomich, and I E Rebrov. Thrust and thrust-to-power ratio in electrohydrodynamic propulsion electrode systems. *Journal of Physics: Conference Series*, 927:012015, nov 2017.

[28] Nicolas Monrolin, Olivier Praud, and Franck Plouraboué. Electrohydrodynamic ionic wind, force field, and ionic mobility in a positive dc wire-to-cylinders corona discharge in air. *Physical Review Fluids*, 3(6), June 2018.

[29] George Matsoukas and Noor Ahmed. Experimental investigation of asymmetrical capacitors for electric propulsion. In *SAE Technical Paper Series*. SAE International, sep 2014.

[30] Rafael Sh Islamov and Yuriy A. Krishtafovich. Erosion and lifetime of tungsten, gold, and nichrome wire anodes in an ultracorona in air. *IEEE Transactions on Plasma Science*, 41(7):1787–1793, jul 2013.

[31] Ian Williams. Ti precision designs: High-side current sensing, 2013.

[32] Nobuhiro Fujioka, Yoshihiro Tsunoda, Akira Sugimura, and Kenji Arai. Influence of humidity on variation of ion mobility with life time in atmospheric air. *IEEE Transactions on Power Apparatus and Systems*, PAS-102(4):911–917, apr 1983.

[33] Bo Zhang, Jinliang He, and Yiming Ji. Dependence of the average mobility of ions in air with pressure and humidity. *IEEE Transactions on Dielectrics and Electrical Insulation*, 24(2):923–929, apr 2017.

[34] Richard G. Stearns. Ion mobility measurements in a positive corona discharge. *Journal of Applied Physics*, 67(6):2789–2799, mar 1990.

[35] J. J. Jones. Electric charge acquired by airplanes penetrating thunderstorms. *Journal of Geophysical Research*, 95(D10):16589, 1990.

[36] P. Cooperman. A theory for space-charge-limited currents with application to electrical precipitation. *Transactions of the American Institute of Electrical Engineers, Part I: Communication and Electronics*, 79(1):47–50, 1960.

[37] James L. Davis and James F. Hoburg. Wire-duct precipitator field and charge computation using finite element and characteristics methods. *Journal of Electrostatics*, 14(2):187–199, aug 1983.

[38] Lin Zhao and Kazimierz Adamiak. EHD gas flow in electrostatic levitation unit. *Journal of Electrostatics*, 64(7-9):639–645, jul 2006.

[39] Alexandre A. Martins and Mario J. Pinheiro. Modeling of an EHD corona flow in nitrogen gas using an asymmetric capacitor for propulsion. *Journal of Electrostatics*, 69(2):133–138, apr 2011.

[40] Alexandre A. Martins. Modelling of an improved positive corona thruster and actuator. *Journal of Electrostatics*, 71(1):61–67, feb 2013.

[41] N. A. Kaptsov. Elektricheskie yavleniya v gazakh i vakuume. *Mosc OGIZ*, 1947.

[42] F. W. Peek. *Dielectric phenomena in high voltage engineering*. CRC press, 1920.